Phase Offsets in the Critical-Current Oscillations of Josephson Junctions Based on Ni and Ni-(Ni_{81}Fe_{19})_{x}Nb_{y} Barriers

B. Baek, M. L. Schneider, M. R. Pufall, and W. H. Rippard

Phys. Rev. Applied **7**, 064013 — Published 12 June 2017

DOI: 10.1103/PhysRevApplied.7.064013

Phase offsets in the critical-current oscillations of Josephson junctions based on Ni and Ni-$(Ni_{81}Fe_{19})_xNb_y$ barriers[a]

B. Baek, M. L. Schneider, M. R. Pufall, and W. H. Rippard

National Institute of Standards and Technology, Boulder, CO 80305, USA

We measure and compare the critical current oscillation characteristics of Josephson junctions as a function of Ni thickness in different barrier structures. The characteristics dependent on the relative Ni thickness, such as the presence of nodes and the oscillation period, are consistent with a conventional, clean-limit magnetic Josephson junction model. However, the oscillation phases have different offsets in the Ni thickness between single Ni and Ni-$(Ni_{81}Fe_{19})_xNb_y$-based barriers, which cannot be explained by the bulk exchange field effect alone. This effect does not originate from the ferromagnetism in $(Ni_{81}Fe_{19})_xNb_y$ nor is it cumulative with an additional $(Ni_{81}Fe_{19})_xNb_y$ layer. Our results present clear evidences that a nonmagnetic layer can affect the superconducting spin phase across the junction as strongly as the conventional exchange field effect.

Superconductor-ferromagnet-superconductor (S-F-S) Josephson junctions (JJs) show unconventional properties based on superconducting spin modulation. In the presence of an exchange field in F, a spin pair $\uparrow$ and $\downarrow$ occupies spin-split Fermi momentum states $\mathbf{k}_\uparrow$ and $\mathbf{k}_\downarrow$ with $\delta k \equiv |k_\uparrow - k_\downarrow| \neq 0$, which results in a finite pair phase $\varphi(x)$ that increases with the distance x from an S-F interface. Consequently, the singlet pair state $\uparrow\downarrow - \downarrow\uparrow$ evolves as $(\uparrow\downarrow - \downarrow\uparrow)\cos\varphi(x) + i(\uparrow\downarrow + \downarrow\uparrow)\sin\varphi(x)$, accompanied by decoherence [1–4]; the pair state oscillates between the conventional singlet $\uparrow\downarrow - \downarrow\uparrow$ and $\uparrow\downarrow + \downarrow\uparrow$ which is one of the triplets ($\uparrow\downarrow + \downarrow\uparrow$, $\uparrow\uparrow$, and $\downarrow\downarrow$). This effect is manifested in the Josephson coupling: I_c oscillates as a function of F thickness and the ground state changes phase between 0 and π across $I_c = 0$ nodes with a node-to-node period of about $\pi\xi_F$, where $\xi_F = 1/\delta k$ [5–8].

New devices based on this effect have been developed to advance superconducting technologies with new functionalities for low-power, high-performance computing [9–11]. Static π phase shifters have been demonstrated for superconducting digital and quantum electronics [12]. With the addition of a second F layer to form a spin valve as the barrier, magnetic JJ memory devices have been developed for switching critical current or phase actively [13–17]. These devices are analogous to a phase shifter for microwave or optical circuits. As a carrier (electron pair) passes through a phase-shifting medium (F), it acquires a constant phase (arctan of the triplet/singlet ratio). If a switchable second phase shifter (second F) is used to add or subtract an additional phase, a switchable phase shifter (spin valve JJ memory) is realized.

Such a simple phase-shifter (SPS) analogy accounts for the bulk effect of the F layer only. Recently, Heim et al. [18] have reported a case with S-I-F-S and S-I-N-F-S (I: insulator, N: normal metal) where different thickness offsets in the critical current oscillation (CCO) result from the subtle differences in the interfacial mismatch in I-F and I-N-F. However, the accompanied experimental result showed a very small difference compared with the oscillation period and a possible difference, e.g., in the magnetic dead layers [19] was not addressed although different dead layers or crystalline structures often originate from different seed layers for the ferromagnetic layer. In this letter, we present our characterization methods and results on magnetic JJs with an embedded Ni layer in different barrier structures including a spin valve. Clearly different phase offsets exist in the CCO curves, which shows a need for further investigation beyond the SPS model.

We sputter-deposit device multilayers, typically substrate/Nb(100)/Cu(5)/M/Cu(20)/Nb(100) (all thicknesses in nanometers in order of growth sequence). M represents magnetic barriers such as a Ni wedge, $(Ni_{81}Fe_{19})_xNb_y$/Cu(5)/Ni wedge, etc. The substrate, a 76 mm diameter Si wafer, is rotated during deposition of every layer other than Ni. The Ni wedge is deposited without substrate rotation, which results in a Ni thickness that varies by a factor of four across the wafer; this method results in a subnanometer resolution for the relative thicknesses at different positions without a stringent control of deposition rate and time. The nonmagnetic spacers of the specified thicknesses are inserted to seed Ni growth and other practical reasons; they are expected to be fully superconducting due to the proximity effect and not alter the superconducting order significantly by themselves.

We fabricate circular or elliptical JJ devices with varying dimensions between 1 μm to 5 μm and aspect ratios between 1:1 to 1:2 using photolithography and etch techniques similar to those used in our previous work [14]. Separately from the fabricated devices, we also measure the saturation magnetic moment of unpatterned Nb(100)/Cu(5)/Ni(d_{Ni})/Cu(20)/Nb(10) multilayers with different Ni thicknesses d_{Ni} at different temperatures. Fig. 1(a) shows that the moment, extrapolated to 0 K, is linear with Ni thickness with an intercept of about 0.7 nm ± 0.07 nm and a slope of 0.5 T, which correspond to the total magnetic dead layer thickness and the saturation magnetization, respectively.

Ni barriers

The magnetization state of the magnetic barriers is a degree of freedom that is not present in conventional, nonmagnetic JJs. Clearly, we need to properly control and characterize the magnetization in order to understand magnetic JJs completely. We use the measurement methods described in ref. 14 and 16 to set the devices at a saturated, single magnetic domain state to prevent complicated nonuniform magnetization states from affecting Josephson property measurements. We carry out magneto-electrical transport measurements on the fabricated devices in liquid helium (4 K) with a conventional dc four-probe setup combined with a superconducting magnet. We apply a high positive in-plane magnetic field ($\mu_0 H \geq 350$ mT) for 5 s to saturate the Ni magnetization along the long axis of the device and then heat the chip for 5 s to untrap flux from the superconducting layers. Subsequently, we measure maximum supercurrents $I_m(H)$ (Fraunhofer pattern [14]) from positive to negative fields. Due to the positively saturated magnetization, the main peak value, the true I_c, is obtained at a negative field [Fig. 1(b)] [14]. At a high enough negative field, the magnetization evolves into hysteretic, intermediate states different from the positively or negatively saturated states and, consequently, $I_m(H)$ deviates from the regular Fraunhofer pattern. We find such a field range with intermediate magnetization by obtaining the field range at which $I_m(0)$ deviates from the value at the saturated state due to the remanent field effect in a JJ; this method is also explained in ref. 16. Such a field range is typically from –40 mT to –200 mT [Fig. 1(c)]. This justifies our choice of saturation field $\mu_0 H \geq 350$ mT and the values of I_c extracted from the main peaks of the Fraunhofer patterns typically at $|\mu_0 H| < 10$ mT.

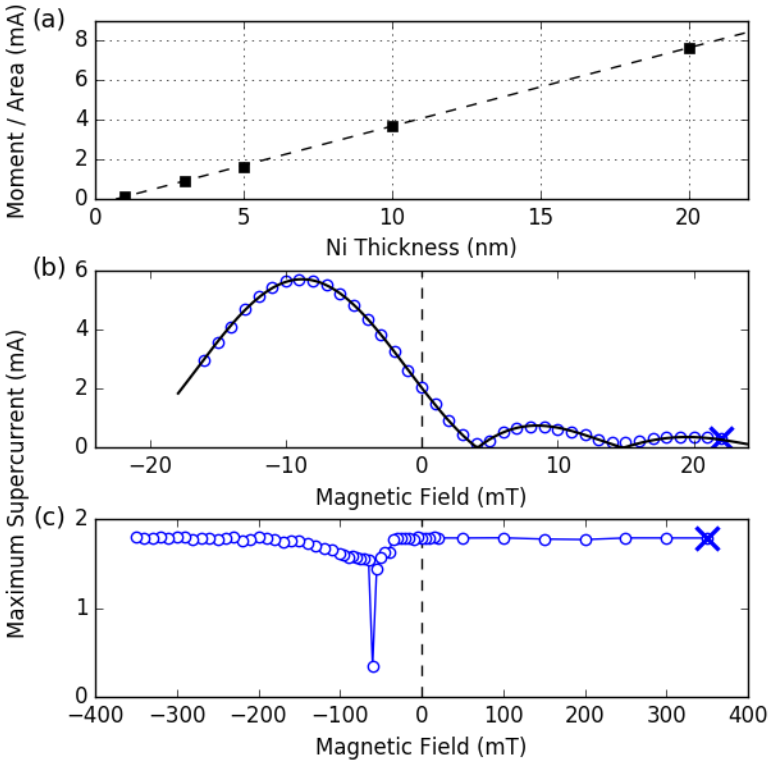

Fig. 1. Basic characterization of single Ni barrier devices. (a) Saturation magnetic moment of unpatterned Ni films obtained with a SQUID magnetometer and extrapolated to 0 K. Dashed line is a linear fit. (b) Typical Fraunhofer pattern from an elliptical (1 μm × 2 μm) Ni barrier JJ at 4 K. Symbols and line are measured data and a fit, respectively. X denotes the start of the sweep. Ni is magnetized with 350 mT prior to the sweep. (c) Typical maximum supercurrent measured at zero field vs. pulsed field amplitude for a Ni barrier JJ at 4 K.

The extracted I_c is normalized with R_n and each data set from two separate wafers is presented in Fig. 2. Although there is a thickness range for which the critical current density J_c is too high to measure, our wedge film method results in dense data points with a small scatter, which reveal clear I_c oscillations with nodes at about 0.9 nm and 3.4 nm to 3.5 nm. This unambiguously confirms CCO purely induced by the exchange field effect in Ni without a parasitic effect from nonuniform magnetization or an uncertainty in the relative F thicknesses in each set of the measured devices. The absolute thicknesses of such thin Ni wedges are reproducible between different wafers to within 5 %.

The measurement results qualitatively follow the clean limit Josephson supercurrent solution in the S-F-S model in ref. [5] (dashed curves in Fig. 2), which is especially characterized by a slow decay compared with typical exponential decays in dirty-limit barriers that have been more widely studied historically. High I_c devices have depressed I_c due to the nonuniform supercurrent distribution associated with the high supercurrent density [20]. By fitting to the theory, we obtain characteristic lengths ξ_{Ni} = 0.93 nm and 0.97 nm with near-zero thickness offsets d_0. From the average ξ_{Ni}, the momentum splitting is $\delta k = \xi_{Ni}^{-1}$ = 1.1 nm^{-1}, which is close to the photoemission result δk = 1.2 nm^{-1} [21]. Thus, the bulk exchange field effect due to Ni is consistent with the basic clean limit theory and our methods are solid. On the other hand, the near-zero d_0 from the fit does not coincide with the estimated magnetic dead layer thickness 0.7 nm obtained from magnetometry measurements [Fig. 1(a)]. This discrepancy may need more detailed investigation of the interfaces but does not affect our main point, which is our focus below.

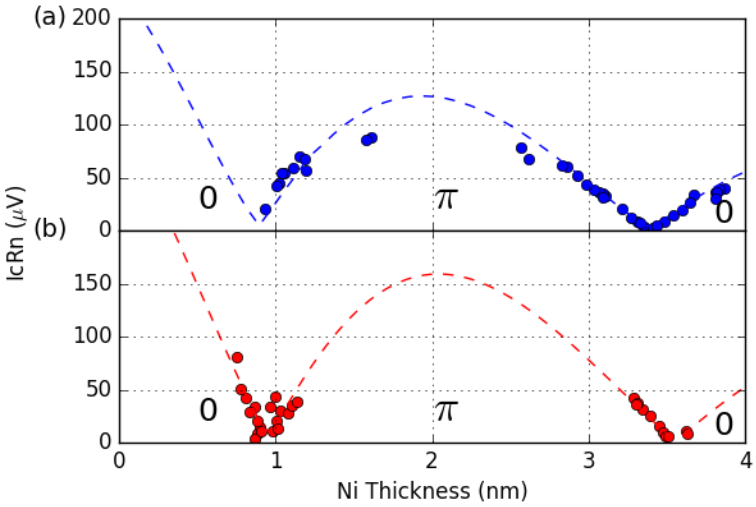

Fig. 2. Ni thickness dependence of the characteristic voltage I_cR_n of single Ni barrier Josephson junctions at 4 K. (a) and (b) are from two different wafers with slightly different Ni thickness ranges. Symbols and curves are measured data and fits, respectively.

Ni-$(Ni_{81}Fe_{19})_xNb_y$ barriers

Similar to ref. 14, we cosputter $Ni_{81}Fe_{19}$ ("NiFe") and Nb for an additional layer $(NiFe)_xNb_y$, which is magnetically decoupled from Ni by Cu(5). With 19 % Nb doping to form a spin valve barrier Ni/Cu/$(NiFe)_{81}Nb_{19}$, $I_m(H)$ becomes hysteretic at a low field range and shows two, partial Fraunhofer patterns corresponding to the parallel and antiparallel magnetization states due to the magnetization reversal of $(NiFe)_{81}Nb_{19}$ around ±4 mT [Fig. 3(a)]. The differences in the offsets and magnitudes of the

two Fraunhofer patterns are due to the remanent and exchange field effects, respectively [14]. With 31 % Nb doping, the ferromagnetic order in $(NiFe)_{69}Nb_{31}$ is reduced below a measurable level as expected from the trend in ref. 14. Consequently, hysteretic spin valve features disappear and $I_m(H)$ becomes similar to those of single Ni devices [Fig. 3(b)].

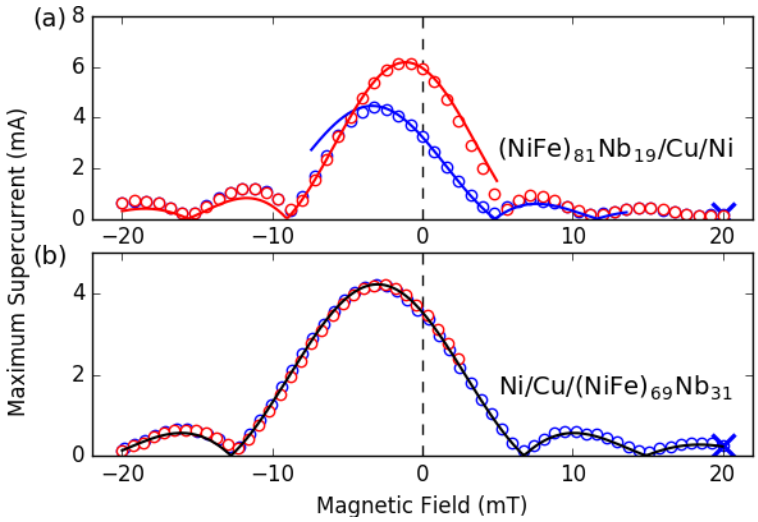

Fig. 3. Fraunhofer patterns at 4 K from devices that contain both Ni and $(NiFe)_xNb_y$ layers. (a) 19 % Nb doping. d_{Ni} = 1.1 nm. (b) 31 % Nb doping. d_{Ni} = 2.3 nm. For each, Ni is positively magnetized prior to the sweep. Symbols and curves are measured data and fits, respectively. Blue and red colors are for downward and upward field sweeps, respectively.

CCO characteristics of Ni and Ni-$(NiFe)_xNb_y$ devices are compared in Fig. 4. Fig. 4(b) shows the two CCO curves each corresponding to parallel (P) and antiparallel (AP) magnetization states, qualitatively similar to the Ni-$(NiFe)_{87}Nb_{13}$ spin valve devices in ref. 14 but with a smaller offset between them due to the weak exchange field and the small thickness in $(NiFe)_{81}Nb_{19}$. According to the SPS model, the baseline Ni CCO curve is straightforwardly extracted by taking the middle-thickness points between the two CCO curves [14, 16] since the free layer should shift the Ni CCO curve by the same effective thickness positively or negatively for the AP or P magnetization, respectively. The resulting first 0-π transition node is near 1.5 nm, which is significantly larger than that of the Ni devices by $0.6\xi_{Ni}$. $(NiFe)_{87}Nb_{13}$ in ref. 14 and our preliminary data from undoped NiFe free layers also show similarly large first node thicknesses. We also note that the spacing between the two nodes is smaller compared with that of Ni devices, which may be due to the crossover from the clean to diffusive regime with a smaller ξ_{Ni} as the Ni layer becomes thicker.

If we consider the very weak ferromagnetic order in 19 % doped layer, such a substantial offset is unlikely to originate from the ferromagnetism in the $(NiFe)_xNb_y$ layer. We further confirm this with a CCO with higher doping of 31 %. Due to the suppressed ferromagnetic order, the device should behave like an S-F-S system with respect to the SPS model but Fig. 4(c) shows the same, large first node Ni thickness as that of the 19 % doping case. Since a Ni deposition is always seeded by 5 nm thick Cu, a significant difference in the dead layers is unlikely to be present and cause such a large offset. We further confirm this point by contrasting the results between Fig. 4(a) and 4(c) which have the same nominal Nb/Cu structure under Ni and should result in the same microcrystalline Cu-Ni interfaces. Fig. 4(d) shows that adding another $(NiFe)_{69}Nb_{31}$ layer on the other side of Ni causes no further change, which indicates the noncumulative nature and irrelevance of the position of the $(NiFe)_xNb_y$ in the barrier multilayer. Interestingly, across all our different barrier structures, the first nodes are at either 0.9 nm or 1.5 nm without intermediate results, as if there were only two possible modes.

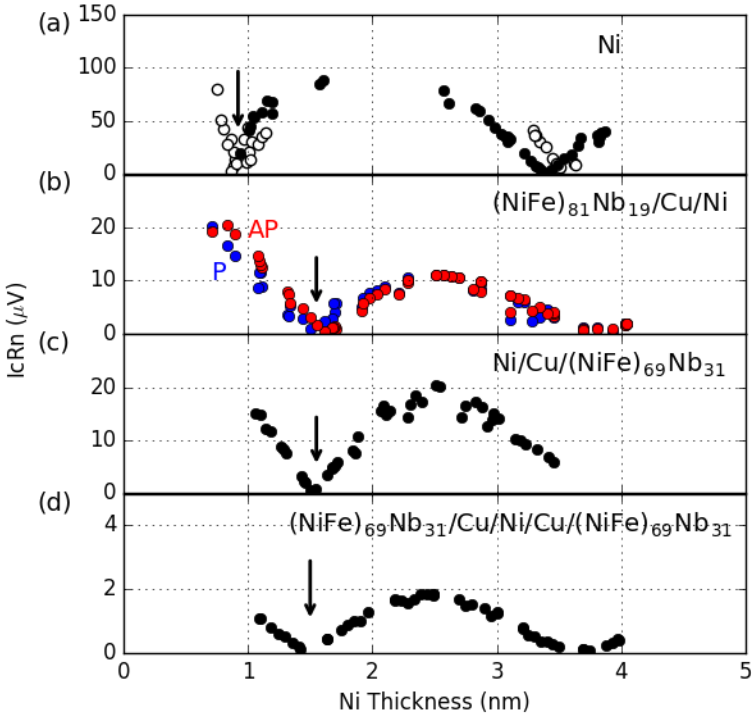

Fig. 4. Comparison of the Ni thickness dependence of I_cR_n between the single Ni and various Ni-$(NiFe)_xNb_y$ barriers at 4 K. Arrows indicate the Ni thicknesses for the first 0-π transition nodes. Barrier structures: (a) Ni, (b) $(NiFe)_{81}Nb_{19}$(1.2)/Cu(5)/Ni, (c) Ni/Cu(5)/$(NiFe)_{69}Nb_{31}$(1.2), (d) $(NiFe)_{69}Nb_{31}$(1.2)/Cu(5)/Ni/Cu(5)/$(NiFe)_{69}Nb_{31}$(1.2). In (a), solid and open symbols represent the

measurement data in Fig. 2(a) and 2(b), respectively. Blue and red colors are for downward and upward field sweeps, respectively.

Discussion

Such unexpected, intrinsic offsets in the CCOs are clear and remarkable. A straightforward ramification is that this effect, of nonmagnetic origin, can be as significant as the bulk exchange field ($0.6\xi_{Ni}$ in the presented case) and should be considered in designing magnetic JJ devices based on the exchange field effect. For example, CCOs separately obtained for both hard and free layers may not be adequate to determine the two operating phase points of a spin valve JJ memory based on these ferromagnetic layers. Instead, a full characterization of the CCO pair such as that shown in Fig. 4(b) may be needed for every material combination.

In relevance to our work, Heim et al. [18] developed a theoretical formulation with different types of nonmagnetic spacers between S and F in S-F-S JJs and showed different phase offsets depending on the interface mismatch or the normal metal thickness. Their theory is based on diffusive transport (dirty limit) throughout the model structures while our structures consist of both ballistic and diffusive layers. Basically, such a ballistic-diffusive hybrid system cannot be described by standard Usadel equations as in the case of Heim et al.'s work. Even if we assume that such a difference does not play a significant role and that the presence of a $(NiFe)_xNb_y$ layer is qualitatively equivalent to the case of a spacer with an increased interface mismatch parameter due to the much higher resistivity of $(NiFe)_xNb_y$ than that of Cu [25], the resulting phase shift is the opposite to our experimental results.

Currently we do not have a satisfactory physical explanation of the effects that we have presented. A potentially relevant phenomenon is the inverse proximity effect. Compared with other ferromagnets of technological importance such as Co, Fe, and NiFe, Ni suppresses the critical current the least [22]. This may indicate that the interface transparency is high, which should also promote the penetration of the magnetic order to the adjacent Cu and Nb [4, 23, 24]. This may result in significant singlet-to-triplet conversion in the nonmagnetic layers. As a result, the effective magnetic thickness is larger and moves the CCO towards the negative direction in thickness. The impact of $(NiFe)_xNb_y$ may be to suppress this effect via the less transparent Cu-$(NiFe)_xNb_y$ interfaces due to its high resistivity [25] or Fermi momentum mismatch, which results in a less negative shift of the CCO. Some calculated CCOs in ref. 26

with different interface transparencies also suggest the possibility of a very small phase transition node thickness associated with highly transparent interfaces. However, such an argument alone does not explain why we do not see a further positive shift with $(NiFe)_xNb_y$/Cu/Ni/Cu/$(NiFe)_xNb_y$ barriers, which should suppress the inverse proximity effect on both sides instead of only one with $(NiFe)_xNb_y$/Cu/Ni barriers.

Another direction to look is the detailed microscopic transport. Systems with large offsets commonly include at least one $(NiFe)_xNb_y$ layer. A JJ with an elemental barrier such as Ni that has a mean free path longer than the layer thickness becomes superconducting via discrete supercurrent-carrying quasiparticle states called Andreev bound states [27]. On the contrary, an alloy layer with an atomically short mean free path should scatter the quasiparticles and result in broad Andreev bound states [28]. Such broad states should be similar to those in S-N-S JJs with a diffusive N barrier except that the bulk exchange field effect still appears in the clean limit ferromagnetic layer (Ni). It is reasonable to connect such a qualitative difference in the microscopic transport mode with a consequent difference in the phase shift. For example, if the broadening is skewed towards either side of the initial discrete energy levels, that should result in an effective phase which induces an offset in the CCO. See, for example, ref. 29 for a basic perspective on the S-F-S transport via Andreev bound states. A future investigation of such microscopic details would improve our understanding of superconducting spin transport in practical devices beyond the idealized models.

Acknowledgment

The authors thank Horst Rogalla and Sam Benz for the helpful discussion and encouragement. We also thank Scott Holmes for commenting on the manuscript. This work was supported by NIST and by the IARPA Cryogenic Computing Complexity (C3) program.

References

[1] P. Fulde, R. A. Ferrell, Superconductivity in a strong spin-exchange field, Phys. Rev. **135**, A550 (1964).

[2] A. I. Larkin, Y. N. Ovchinnikov, Nonuniform state of superconductors, Sov. Phys. JETP **20**, 762 (1965).

[3] E. A. Demler, G. B. Arnold, and M. R. Beasley, Superconducting proximity effects in magnetic metals, Phys. Rev. B **55**, 15174–15182 (1997).

[4] M. Eschrig, Spin-polarized supercurrents for spintronics, Phys. Today **64**, 43–49 (2011).

[5] A. I. Buzdin, L. N. Bulaevskij, and S. V. Panyukov, Critical-current oscillations as a function of the exchange field and thickness of the ferromagnetic metal (F) in an S-F-S Josephson junction, J. Exp. Theor. Phys. Lett. **35**, 178–180 (1982).

[6] V. V. Ryazanov, V. A. Oboznov, A.Yu. Rusanov, A.V. Veretennikov, A. A. Golubov, and J. Aarts, Coupling of Two Superconductors through a Ferromagnet: Evidence for a π Junction, Phys. Rev. Lett. **86**, 2427-2430 (2001).

[7] T. Kontos, M. Aprili, J. Lesueur, F. Genêt, B. Stephanidis, and R. Boursier, Josephson junction through a thin ferromagnetic layer: negative coupling, Phys. Rev. Lett. **89**, 137007 (2002).

[8] A. I. Buzdin, Proximity effects in superconductor-ferromagnet heterostructures, Rev. Mod. Phys. **77**, 935976 (2005).

[9] K. K. Likharev and V. K. Semenov, RSFQ logic/memory family: a new Josephson-junction technology for sub-terahertz-clock-frequency digital systems, IEEE Trans. Appl. Supercond. **1**, 328 (1991).

[10] O. A. Mukhanov, Energy-Efficient Single Flux Quantum Technology, IEEE Trans. Appl. Supercond. **21**, 760–769 (2011).

[11] D. S. Holmes, A. L. Ripple, and M. A. Manheimer, Energy-efficient superconducting computing—power budgets and requirements, IEEE Trans. Appl. Supercond. **23**, 1701610 (2013).

[12] A. K. Feofanov, V. A. Oboznov, V. V. Bol'ginov, J. Lisenfeld, S. Poletto, V. V. Ryazanov, A. N. Rossolenko, M. Khabipov, D. Balashov, A. B. Zorin, P. N. Dmitriev, V. P. Koshelets, and A. V. Ustinov, Implementation of superconductor/ferromagnet/superconductor π-shifters in superconducting digital and quantum circuits, Nat. Phys. **6**, 593–597 (2010).

[13] C. Bell, G. Burnell, C. W. Leung, E. J. Tarte, D.-J. Kang, and M. G. Blamire, Controllable Josephson current through a pseudospin-valve structure, Appl. Phys. Lett. **84**, 1153–1155 (2004).

[14] B. Baek, W. H. Rippard, S. P. Benz, S. E. Russek, and P. D. Dresselhaus, Hybrid superconducting-magnetic memory device using competing order parameters, Nat. Commun. **5**, 3888 (2014).

[15] M. A. E. Qader, R. K. Singh, S. N. Galvin, L. Yu, J. M. Rowell, and N. Newman, Switching at small magnetic fields in Josephson junctions fabricated with ferromagnetic barrier layers, Appl. Phys. Lett. **104**, 022602 (2014).

[16] B. Baek, W. H. Rippard, M. R. Pufall, S. P. Benz, S. E. Russek, H. Rogalla, and P. D. Dresselhaus, Spin-transfer torque switching in nanopillar superconducting-magnetic hybrid Josephson junctions, Phys. Rev. Appl. **3**, 011001 (2015).

[17] E. C. Gingrich, B. M. Niedzielski, J. A. Glick, Y. Wang, D. L. Miller, R. Loloee, W. P. Pratt, and N. O. Birge, Controllable 0–π Josephson junctions containing a ferromagnetic spin valve, Nat. Phys. **10**, 1038 (2016).

[18] D. M. Heim, N. G. Pugach, M. Yu Kupriyanov, E. Goldobin, D. Koelle, R. Kleiner, N. Ruppelt, M. Weides, and H. Kohlstedt, The effect of normal and insulating layers on 0-π transitions in Josephson junctions with a ferromagnetic barrier, New J. Phys. **17**, 113022 (2015).

[19] J. W. A. Robinson, S. Piano, G. Burnell, C. Bell, and M. G. Blamire, Critical Current Oscillations in Strong Ferromagnetic π Junctions, Phys. Rev. Lett. **97**, 177003 (2006).

[20] R. A. Ferrell, Josephson tunneling and quantum mechanical phase, Phys. Rev. Lett. **15**, 527–529 (1965).

[21] D. Y. Petrovykh, K. N. Altmann, H. Höchst, M. Laubscher, S. Maat et al., Spin-dependent band structure, Fermi surface, and carrier lifetime of permalloy, Appl. Phys. Lett. **73**, 3459 (1998).

[22] B. Baek, M. L. Schneider, W. H. Rippard, and M. R. Pufall, Switchable Josephson junctions with Fe/Cu/Ni and Co/Cu/Ni spin-valve barriers, Applied Superconductivity Conference 2016, Denver, CO.

[23] P. M. Tedrow and E. Tkaczyk, Spin-Polarized Electron Tunneling Study of an Artificially Layered Superconductor with Internal Magnetic Field: EuO-Al, Phys. Rev. Lett. **56**, 1746–1749 (1986).

[24] J. Xia, V. Shelukhin, M. Karpovski, A. Kapitulnik, and A. Palevski, Inverse Proximity Effect in Superconductor-Ferromagnet Bilayer Structures, Phys. Rev. Lett **102**, 0870024 (2009).

[25] M.-M. Chen, N. Gharsallah, G. L. Gorman, and J. Latimer, Ternary NiFeX as soft biasing film in a magnetoresistive sensor, J. Appl. Phys. **69**, 5631–5633, (1991).

[26] Z. Radović, N. Lazarides, and N. Flytzanis, Josephson effect in double-barrier superconductor-ferromagnet junctions, Phys. Rev. B **68**, 014501 (2003).

[27] A. F. Andreev, The thermal conductivity of the intermediate state in superconductors, Sov. Phys. JETP **19**, 1228 (1964).

[28] S.-K. Yip, Energy-resolved supercurrent between two superconductors, Phys. Rev. B, **58**, 5803–5807 (1998).

[29] H. Sellier, C. Baraduc, F. Lefloch, and R. Calemczuk, Temperature-induced crossover between 0 and π states in S/F/S junctions, Phys. Rev. B **68**, 054531 (2003).